Dislocation microstructure of 4H-Silicon Carbide plastically deformed around its transition temperature

A. Lara[a], M. Castillo-Rodríguez[b,*], A. Muñoz[a] and A. Domínguez-Rodríguez[a]

[a]Departamento de Física de la Materia Condensada, Facultad de Física, Universidad de Sevilla, Apartado 1065, 41012 (Sevilla), Spain

[b]Max Planck Institute for Metals Research, StEM, Heisenbergstr. 3, 70569 Stuttgart, (Germany)

[b]castillo@mf.mpg.de

Abstract: 4H-SiC samples have been plastically deformed by basal slip activation at temperatures between 800°C and 1300 °C. Experimental results show two regimes characterized by a mechanical behavior substantially different. These two different behaviors have been already observed, and a transition temperature was established around 1030 °C. However, we find that this transition temperature is not so well defined since these two mechanisms are observed to be co-operating together between 1000°C and 1100 °C. Samples deformed at different temperatures were investigated by means of the complementary use of transmission electron microscopy and high resolution techniques. Here we study dislocation microstructure to identify the mechanism that governs the plasticity of this material in each regime. Dissociation of basal dislocations takes place along the whole temperature range investigated, but its influence on the dislocation motion is different in each regime. In the high temperatures regime, after dissociation both partials slip together in the basal plane bordering a stacking fault. By standard stereography projections we determined the dissociation width and the elasticity theory provides a stacking fault energy value is 20±5 mJ/m^2. However, below the transition temperature the difference in mobility of partials, together with the low stacking fault energy value, allow the leading partials to escape from its companion. Here we discuss about the consequences of this fact on the crystal structure (nucleation of 3-cubic bands) and on its mechanical behavior (high work-hardening rate). Also we deal about basal dissociated dislocations forming dipoles and the influence of each regime on their final configuration.

* Corresponding author. Tel.: +49 (0) 711 689-3583; fax: +49 (0) 711 689-3522.
E-mail address: castillo@mf.mpg.de (M. Castillo-Rodríguez).

Keywords: 4H-SiC, TEM, mechanical properties, ceramics, dislocations.

1. Introduction.

Silicon carbide is one of the most important ceramic due to its excellent mechanical behavior at high temperature together with a wide-band-gap semiconductor [1], leading to a widespread technological use. The existence of a numerous polytypic forms of this material makes it even more interesting from a theoretical and technological point of view. Indeed, there are a lot of studies and theories to explain the occurrence of polytypism in SiC [2-4], and in particular the possibility of a local transformation inside the matrix which could affect the initial properties of the material [5-11]. This transformation has been previously observed in 4H-SiC single crystal polytype during different process: i) by thermal oxidation [12], ii) by annealing in Ar for 90 min at 1150 ºC [13] and also iii) by stress induced at temperatures between 400 ºC and 700 ºC [14]. In all cases, transmission electron microscopy reveals stacking faults and local bands of 3C polytype in the 4H-SiC matrix. On the other hand the occurrence of this phenomenon has a strong influence on the plasticity of this material, since it was reported by Demenet et al. [15] that this material exhibits two different regimes characterized by a different mechanical behavior, separated by a transition temperature T_c of about 1030 ºC.

In this context, we have performed some compression tests around the transition temperature, in order to study the dislocation microstructure to get information about the deformation mechanism operating in each regime. The present work is mainly focused on the analysis of samples after deformation by means of weak-beam dark-field (WB-DF) imaging and high-resolution TEM (HRTEM) observations. Mechanical results are going to be reported afterwards.

2. Experimental procedure.

Quadrangular prisms (5,5 x 2,7 x 2,7 mm^3) of 4H-SiC were deformed in compression. The specimens were oriented by Laue back reflection such that the compression axis lies in the $\{11\bar{2}0\}$ plane at 45º from [0001] direction. This orientation activates $(0001)1/3\langle 11\bar{2}0\rangle$ slip system with a Schmid factor of 0.5. Samples were prepared by sawing and grinding and all side faces were polished to avoid crack initiation. The tests

were performed with a constant displacement rate (initial strain rate of $1{,}5 \cdot 10^{-5}$ s^{-1}) in air at temperatures between 800 ºC and 1300 ºC. After plastic straining, light-optical micrographs using polarized light attested the activation of the (0001)1/3<11 $\bar{2}$ 0> basal slip system. Specimens for transmission electron microscopy (TEM) were prepared parallel to the slip plane for weak-beam dark-field (WB-DF) imaging and perpendicular to the slip plane to perform high-resolution TEM (HRTEM) observations. TEM specimens were prepared by standard procedures involving grinding, dimpling, polishing, and ion milling in a Gatan precision ion-polishing system. Dislocation microstructure was investigated by WB-DF in a Philips CM200 microscope, operating at 200 kV, which allows large tilts. For HRTEM observations, a JEOL JEM-4000EX microscope with a point resolution of 0.17 nm was used, operating at 400 kV.

3. Results and discussion.

As it is observed from mechanical tests, silicon carbide 4H deformed by basal slip shows a transition temperature Tc between 1000°C and 1100 ºC that separates two regimes in which the mechanical behavior exhibits clear differences (detailed information about mechanical results will be reported in the future work). This transition was previously reported by Demenet et al. [15]. Since plastic deformation of single crystals is due to the movement of dislocations, we have performed a study of the dislocation microstructure to get information to justify the mechanical behavior of this material. This study has been carried out by means of two complementary techniques of transmission electron microscopy. For one hand weak beam technique to study the general organization of the dislocations in their slip plane, and on the other hand high resolution transmission electron microscopy to analyze configurations at atomic scale, like possible changes in the stacking plane sequence, and also to study the dislocation core. We have selected samples deformed at temperatures above (1300 °C), below (900 ºC) and close (1100 and 1000 °C) to the transition temperature.

3.1 Above the transition temperature.

The figure 1 shows the microstructure of dislocations of a sample deformed by basal slip at 1300 º C. Looking at the diffraction pattern at the bottom, it is easy to verify that dislocation lines are arranged along simple crystallographic directions, indicating that

Peierls mechanism controls the dislocations glide. On the other hand, basal dislocations are dissociated into two partials bordering a stacking fault SF according to:

$$1/3<\bar{1}2\bar{1}0> \longrightarrow 1/3<\bar{1}100> + SF + 1/3<01\bar{1}0> \quad (1)$$

At the top of the figure 1 we can see one basal dissociated dislocation which is isolated, i. e. it is not composing a dipole with another dislocation. The insert at its left shows the fringes coming from the staking fault (since **g.b** is not an integer). In this configuration, partials are quite straight and their separation of about 30 nm remains almost constant (see also partials of figure 2). However, at the center of figure 1 we observe couples of partials forming dipoles. The stacking fault is displaying fringes in the insert at its right. Moreover, the inserts at the top center and right taken under different g reflections show the intensity extinction of each partial, and reveal that in this configuration one couple of partials have straight dislocation lines separated by 50 nm, which is a bit bigger than in case they were isolated. The situation for the other couple of partials is different, since one partial is straight but its companion is zigzagged producing a high fluctuation of the dissociation width between 50 and 115 nm. A possible explanation is given through this paper.

The stacking fault plane seems to be close to the basal plane, since tilting around the dislocation line we observe that the dissociation width decrease as soon as we leave the basal plane. To further characterize dissociation properties in this material, we have conducted a dedicated determination of the stacking fault habit plane and of the dissociation width for the two couples of partials in figure 2. This was achieved by tilting around the dislocation line direction, which coincides with $\mathbf{g} = 1\bar{2}10$ and taking micrographs at different orientations. Taking into account the angle tilted at the microscope, and using the Wulff's network together with the stereography projection we have determined the angle θ between the electron beam and the [0001] direction for each orientation. Also we have measured the dissociation distance d between the images of the two partial dislocations. Note that this distance d is not the real distance between partials, but the distance between partials projected in the plane perpendicular to the electron beam. On the other hand, it is worth emphasizing that the dislocation signal is originated from a region in the core vicinity adequately distorted to satisfy the Bragg orientation, off the actual dislocation line position. Furthermore, since partials have

non-parallel Burgers vectors they are viewed under distinct **g·b** conditions and their images are thus shifted differently with respect to the actual positions of the partials depending on the sign of the product s_g **g·b**. This property has introduced the more uncertainty contribution to the calculation of the stacking fault habit plane and the dissociation width.

Table 1 shows the distance *d* between the images of partials for various electron beam orientations θ, corresponding to the two dissociated basal dislocations in figure 2.

The real dissociation width *h* and the angle β between the stacking fault habit plane and the [0001] direction are related to *d* and θ by the following expression [16]:

$$Cos\left(ArcCos\left(\frac{d}{h} \right) + \beta \right) = Sen\,\theta \qquad (2)$$

Then, from a least-square fit of expression (2) to the various (θi, di) pairs measured experimentally we obtain β and *h* values (table 2). In both cases, the stacking fault habit plane is close to the basal plane with partials separated by 30 nm. Then, dissociation seems to takes place by glide. All these results are coherent with what other authors have previously reported [15].

Once that dissociation process has been characterized and it is known the dissociation width and the stacking fault habit plane, it is possible to estimate the stacking fault energy γ contained between partials. The repulsive force between partials is balanced by the stacking fault generated in between, so taking into account their expressions [17] one obtains that the stacking fault energy γ is given by:

$$\gamma = \frac{\mu b^2}{2\pi s}\left(Cos^2[\psi] + \left(\frac{1}{(1-\nu)}\left(Sen^2[\psi] + (2\,Sen[\psi]\,Sen[\alpha]\,Cos[\alpha])\right)\right)\right) \qquad (3)$$

where μ = 159 GPa [18] is the shear modulus, ν is Poisson's modulus with a value of 0.25, ***b*** is Burgers vector of the partial dislocation and ψ its character, *s* is the dissociation width and α is the angle between the stacking fault plane and the slip plane. Then, if we consider the two configurations in figure 2, where the screw basal dislocations 1 and 2 are glide-dissociated (α =0 º) into two partial dislocations (ψ =30 º)

separated by $s = h = 32 \pm 4$ nm (table 2) then we obtain $\gamma = 20 \pm 5$ mJ/m2. This value is in good agreement with results obtained by different authors. Hong and cabbage, [19] reported a value of $\gamma = 14.7 \pm 2.5$ mJ/m2. On the other hand, based on a theoretical model (ANNNI) it is found that the stacking fault energy must be comprised between 19.1 y 27.2 mJ/m^2 [21, 22]. So that, the value we have obtained is quite satisfactory since it is inside the error bar of both of them.

Figure 3 is a high resolution micrograph of the sample 4H-SiC deformed by basal slip at 1300 ºC. In this micrograph we observe a bright contrast of about 30 nm in length contained in the basal plane. This contrast could come from the stacking fault contained between partial dislocations, which are at the edges marked by arrows in figure 3. This is in good agreement with results obtained by weak beam for the dissociation process, in which we obtained that the dissociation plane was close to the basal plane and the dissociation width was approximately 30 nm, and then supporting this assumption.

Figure 3.b magnifies the zone of the black arrow in figure 3.a. The projection of every atom column in the $\{\bar{2}110\}$ plane generates every black dot that is observed in the micrograph. The resolution of the microscope is not high enough to distinguish between the C and Si atoms. In fact, as we see in figure 3.b, this projection does not have spherical shape but they are elongated due to the overlapping of both Si and C atom columns, and depending on their relative positions they are elongated in one or another direction. Since the sequence of Si stacking planes in the 4-H structure is ...CABACABAC…, where the repeating sequence involves four planes, and for the C one is …αβγ…, only comprising by three planes, and since it is not possible to solve the structure Si-C, the stacking sequence that it is observed in the micrograph must be the one comprising the highest number of planes in the repeating sequence, so the Si one. We have enlarged every micrograph to be able to determine properly the stacking sequence of each atom row. Analyzing the stacking sequence on the right of the black arrow (figure 3.b), where the partial dislocation has not slipped yet, we can verify that there is no change in the stacking fault sequence. In this region the SiC structure is the 4H (figure 3.b). However, if the analysis is performed on the left side, where the partial has slipped, it is observed a change ACAB→BACA in the stacking fault (see sequence showed in figure 3.b).

3.2 Below the transition temperature.

The dislocation microstructure below the transition temperature is composed by partial dislocations originated by the dissociation process of eq. (1). At this temperature (900 °C) it is observed that both partials do not glide together and only one of them glide in the basal plane. These results agree with those found by Pirouz's analysis [15]. Nevertheless, the partial dislocation that is observed does not have always the same Burgers vector, as we verifies in the insert of in the micrograph 4, where using g = $11\bar{2}0$ only the dislocation number 5 is extinguished and therefore its Burgers vector is b=1/3 $[1\bar{1}00]$. This differs from [20] since they observed always the same Burgers vector for partial dislocations and then they postulated a possible difference in the mobility between the leading and the trailing partial to justify their observation. They argue that the core of one partial should be richer in silicon and its companion in carbon leading to a different activation barrier for nucleation and having the former more mobility than the latter. It is worth emphasizing that in their observations all basal dislocations have screw character giving 30° mixed partials after dissociation. However, in figure 4 one can observe all characters for $<1\bar{1}00>$ partials. For instance, dislocations 5, 8 and 11 are screw, 30° mixed and 60° mixed respectively. Different dislocation character must lead to different C-Si ratio at the dislocation core and consequently to a different dislocation mobility, explaining why we do not find that all partials have the same Burgers vector like in [15].

Moreover, apart of the contour lines, it is observed a sort of bands at the background of the micrograph which are even much more defined at the insert under g=$11\bar{2}0$ conditions. These bands, absents in the micrographics of the sample deformed at 1300 °C, might be related to the stacking fault produced in the material when only the leading partial dislocation slips.

High resolution micrographs of samples deformed at 900 °C display clear differences with samples deformed at 1300 °C. In fact, those different contrasts of 30 nm in length contained in the basal plane frequently found at 1300 °C are no longer observed at 900 °C. Instead of them, many bands appear (figure 5), whose analysis is discussed below.

At the top of figure 5 we observe pairs of planes with dark contour, corresponding to the C and A stacking plane sequence of Silicon, where the atom columns are very well

defined, followed by pairs of planes with brighter contour, related to the B and A stacking plane sequence of Silicon, where atom columns are worse defined. The repetition of these two couples of planes generates the structure of 4H-SiC that we observe at the top and at the bottom of figure 5. Nevertheless, there are some bands (B in figure 5) in which this sequence is changed. In micrograph 6, which is a magnification of one of these bands, we have performed an analysis of the stacking plane sequence along the [0001] direction. Starting from de top, we go down along the direction [0001] until we find the first change in the stacking sequence. This sequence should be "A^1" but instead it is "C". This change in the stacking plane sequence cannot take place after the glide of both partial dislocations, because the change of the stacking sequence produced after the glide of the leading partial is removed by the glide of the trailing partial. So, this change only can take place due to the glide of a 1/3 $<1\bar{1}00>$partial dislocation, which generates a region where the part of the crystal below the slip plane is displaced, with regard to the above area, a distance equivalent to the projection of its Burgers vector in the observation plane.

Then, one can imagine that among sequences "A^1" and “B” one leading partial has glided producing a shift between the parts above and below. For simplicity we consider that the part above remains equal and it is the part below the one which is shifted. So now A^1" is "C", and the stacking plane sequence of all planes below is also changed after this shift, that we display in the second column. Afterwards, this process could take place between sequences "A^2" and “B” and "A^3" and “B”, generating the sequence described on the third column. Again between "A^4" and “B” it is produced the glide of one partial and the final stacking plane sequence shown to the right. At the end of the whole process, a 3C band is originated in the 4H material. It worth emphasizing that this band could be created by the glide of different partials like in "A^2" and “A^3”or by means of the cross-slip of the same partial, that probably occurs in "A^1" and “A^2”.

3.3 Close to the transition temperature.

Figure 7 shows the dislocation microstructure of a 4H-SiC sample deformed by basal slip at 1100 ° C. It is possible to observe cases (marked with the letter D) in which both leading and trailing partial dislocations, produced after the dissociation of basal

dislocations, slip together and cases where only the leading partial dislocation slips (L) without its companion.

The stacking fault fringes (SF) are observed clearly in the inserts on the right, since the scalar products $\mathbf{g}\cdot\mathbf{b_1}$ and $\mathbf{g}\cdot\mathbf{b_2}$ (with $\mathbf{b_1}$ =1/3[$\bar{1}$100] and $\mathbf{b_2}$ = 1/3[01$\bar{1}$0]) are not an integer and therefore between the images of the dislocation lines it is possible to these fringes. In figure 8 we show a scheme of the central top insert of micrograph 7 in which there are some reactions between partial dislocations. In black is represented the basal perfect dislocation **b**=1/3[$\bar{1}$2$\bar{1}$0] which is dissociated into $\mathbf{b_1}$ = 1/3[$\bar{1}$100] (in blue) y $\mathbf{b_2}$ = 1/3[01$\bar{1}$0] (in red). In the central part of this configuration has taken place the annihilation of partial dislocations with opposite Burgers vectors $\mathbf{b_1}$ = 1/3[$\bar{1}$100] (in blue), which had screw character and have cross-slipped and annihilated mutually (the remaining pair of partial dislocations is marked in red).

Dislocation microstructure is quite similar in samples deformed at 1000 °C (figure 9) and at 1100 °C (figure 7). At 1000 °C it is found a mixture of what we have observed below and above the transition temperature. We observe in cases in which both partial dislocations slip together after basal dissociation (D in figure 9) and also cases in which the leading partial slips alone (L in figure 9). The former case can be observed in the top right insert of figure 9. It has been taken using g = $\bar{2}$110 reflection and clearly shows the extinction of one partial, the one with **b**=1/3[01$\bar{1}$0], whereas its companion with **b**=1/3[$\bar{1}$100] is visible. On the other hand, in the two others inserts, taken also with g = $\bar{2}$110, all dislocations of the area are extinguished, indicating that they all have the same Burgers vector (**b**=1/3[01$\bar{1}$0]) and are slipping without their respective companions. Both mechanisms operate at 1100 °C and 1000 °C, so we find that the transition is not abrupt, whose temperature value estimated by Demenet et al. [15] was $T_c \approx 1030°C$, but there is a temperature range around Tc in which both mechanisms coexist. This range according to our observations is comprised between 1000 °C and 1100 °C. Furthermore, depending on the temperature one mechanism prevails on the other one. Note that at 1100 °C (figure 7) there are much more partial pairs than leading partials slipping alone. However, at 1000 °C (figure 9) the situation is the opposite. It is worth emphasizing that again in samples deformed at both 1000 and 1100 °C one can observe the sort of bands at the background of the micrograph which were observed in

samples deformed at 900 °C but absents at 1300 °C. Then they are a clear evidence of the low mechanism operation, as we found in samples deformed at 900 °C.

Samples deformed at temperatures close to the transition temperature have been studied by high resolution. As we have seen by weak beam-dark field imaging the dislocation microstructure at these temperatures is a mixture of what we had observed for temperatures above and below the transition temperature. Then, we expect that high resolution micrographs contain also elements from both regimes. Figure 10 shows some bands of different contrast that background (B in the figure 10), parallel to the basal plane and occupying the whole width of figures. These bands are typically observed in high resolution micrographs of samples deformed below the transition temperature (figures 5 and 6), whose structure is cubic as we have showed. Nevertheless, the band's number is much less at 1100 ºC than at 900 °C. This is coherent with the fact that when the temperature increases from 900 °C to 1100 °C the mechanism operating at lower temperatures loses relevancy with regards to the higher temperature mechanism, until it is no longer activated at 1300 °C, as we have experimentally observed in weak beam micrographs.

On the other hand, another different contrasts are observed (D in the figure 10), also contained in the basal plane but with a much smaller width, of approximately 30 nm. These contrasts are observed in samples deformed above the transition temperature (figures 3), which come from the stacking fault contained between partial dislocations. The dissociation width is approximately the same at 1300°C than at 1100 °C, evidence that the stacking fault energy is constant in this range of temperatures. However, when two dissociated basal dislocations are forming a dipole, the dissociation width is strongly modified. We discuss this dipolar effects on dissociation process in the next section.

3.4 Dipolar effects on dissociation process.

Figure 10.c shows a configuration where two basal dislocations, lying in different but close basal planes, are dissociated by glide into two partials. It is remarkably that the dissociation width is perceivably decreased from 30 nm in case of an isolated

dissociation process to 18 nm in this dipolar configuration. This fact is an evidence of the strong dipole effect on dissociation. The reason easily shows up examining the forces acting in such a dipolar configuration (figure 11). First, there is a repulsive interaction force, F^R, between partials which is balanced by the stacking fault generated between them, F^{γ}. Secondly, in the case of dipoles the partials bordering one stacking fault interact with the partials bordering the other fault. Because the two dissociated dislocations of a dipole have anti-parallel Burgers vectors they attract each other by the interaction force, F^I. Then, it is clear that this attractive force F^I is responsible for the smaller dissociation width observed in this dipolar configuration.

Moreover, owing to F^I it is established a relationship between dissociation width and dipole high since this force depends on the separation between partials. Since partials have non screw character, they cannot change their slip plane by cross slip to mutually annihilate, except by atomic diffusion processes that requires higher temperatures than those studied in this work. So, only its component in the basal slip plane has some influence on the equilibrium separation between partials. This sort of configuration has been also found in others material, like in perovskites [23]. This separation can be calculated taking expressions 5-17 and 5-18 of Ref. [17] for the forces and making the force balance $F^R - 2F^I - F^{\gamma} = 0$, what leads to the following expression:

$$\frac{\mu b^2}{2\pi s}\left(Cos^2[\psi]+\frac{Sen^2[\psi]}{(1-\nu)}\right)-2\frac{\mu b^2}{2\pi\sqrt{s^2+d^2}}\left(Cos^2[\psi]+\frac{Sen^2[\psi]}{(1-\nu)}\right)-\gamma=0 \qquad (4)$$

where *s* and *d* are the dissociation width and the dipole height, respectively. The most frequently observed case corresponds to a screw basal dislocation which dissociates into two partial mixed (ψ = 30°). Taking the stacking fault energy γ= 20 ± 5 mJ/m^2, calculated in section 3.1, and a dipole height d = 18 ± 2 nm from the micrograph 10.c we obtain that the dissociation width is s = 9 ± 2 nm. This result is in good agreement with the dissociation width 10 ± 2 nm measured in the micrograph. It is worth emphasizing that the dipolar effect on dissociation will decrease rapidly as the dipole height increases. This is because the force F^I is inversely proportional to the partial separation, so it is expected that when the dipole height is much greater than the dissociation width this dipolar effect will be negligible and the equilibrium separation between couple of partial will be practically the same as in the case they are isolated.

However, we also have observed dipolar configuration where the dissociation width is much larger than for an isolated case (see figure 1). Indeed, in samples deformed at 1300 °C is observed that one partial is zig-zagged and the dissociation width fluctuates surprisingly, so much that the dissociation width is sometimes almost three times longer. Figure 12 is a high resolution micrograph in which displaying one of these dipolar configuration where the dissociation width is approximately twice than its normal value. Figure 13 shows the in stacking plane sequence on the left and on the right sides of the black arrow of figure 12. On the right side, the stacking plane sequence remains unaltered, but as one can see on the left side there is a change due to the partial glide. This fact in principle seems to be contradictory with the results of dipole analysis of figure 10.c, where due to the force F^I dissociation width decreases owing to the dipolar effect.

However, there is a difference between the dipole of figure 10.c and figure 12. The dipole height for the former is approximately 18 nm whereas for the latter is about 60 nm. This difference in the dipole height could explain the surprising dissociation width of the dissociation shown in figure 12. The stability of a dipole depends on its height and the applied stress, and there is a critical height value d_c where for longer height the dipole becomes unstable and the applied stress is able to break the dipole. This is because the resolved applied stress is stronger than the attractive interaction between dislocations. This critical height value d_c must verify the following expression [17]:

$$\frac{\mu b^2}{2\pi s}(Cos^2[\psi]+\frac{Sen^2[\psi]}{(1-\nu)})-\frac{\mu b^2}{2\pi\sqrt{s^2+d_c^{\,2}}}(Cos^2[\psi]+\frac{Sen^2[\psi]}{(1-\nu)})-\gamma \geq \tau^* b \qquad (5)$$

where τ^* is the stress applied on dislocations, i.e. the resolved shear stress τ minus the tension due to friction network τ^0. Considering the case of a screw basal dislocation dissociates into two mixed partial (ψ = 30 °), taking the stacking fault energy value calculated above γ= 20 ± 5 mJ/m^2 and from experimental curves taking τ^* = 1 MPa, we find that from 50 nm dipoles are no longer stable. This result indicates that the dipole in figure 10 is stable, whereas the one in micrograph 12 is unstable whose height is about 60 nm. This could explain the bigger dissociation width exhibited by the latter. Since the dipole is unstable, the resolved applied stress to the partial resolved is bigger than the attractive interaction coming from the other couple of partials so that the dipole is breaking. However, this breaking up may affect differently to each partial. The

attractive interaction from the other pair of partial could increase the difference in mobility between the leading and the trailing partial. Thus, when the dipole is breaking, this major difference would allow the leading partial dislocation to be further separate from the trailing partial and then increases the dissociation width.

3.5 Correlation between dislocation microstructure and mechanical behavior.

The mechanical behavior of 4H-SiC is characterized by two different regimes [15]. In the low temperature one, this material does not exhibit the yield point and quickly it is work hardened. Nevertheless at higher temperatures, the yield point is clearly observed and the work hardening is practically inexistent. These differences evidently obey to a change in the deformation mechanism. According to literature, the mobility of a partial dislocation depends on the dislocation core, and in this case can be richer in Carbon or in Silicon, being the latter the one with major mobility [15]. When the temperature is high enough to activate diffusion processes the difference in mobility is not significant and both partial dislocations slip relatively together, as we have seen in micrographs of samples deformed above the transition temperature. Then, if we consider a Frank-Read's source of basal dislocations (figure 14), since both partial dislocations glide together then the final situation is the emission of both partials, with a stacking fault in between, and the source can emit more couple of partials in the same slip plane. So, the fact that the source is dissociated does not have any effect in its operability and therefore the yield point is expected, because it is due to readjustments between the dislocation density, their velocity and the strain rate of the mechanical tests. Furthermore, dissociation does not produce work hardening is due to the dipole formation which impede the glide of the other dislocations. Since they are unstable above a relatively low height, 50 nm, as we have calculated in previous section, it is expected an insignificant work hardening as observed in mechanical tests.

On the other hand, if temperature is not high enough the trailing partial (in red in figure 15) has serious difficulties to slip together with the leading partial (in blue), which has much more mobility. So finally, only the leading partial is emitted. However, owing to the stacking fault generated by the partial glide (grey area); it is not possible to return to emit again same partial [15]. Moreover, after this emission the situation is the opposite,

i.e., the leading partial is now behind the trailing partial. Between both partial dislocations there is a repulsive force that in absence of stress would make them to be separated a distance *d*, for which this force cannot overcome the lattice friction. Nevertheless, due to the applied tension this distance is smaller, leading to an increase in the energy of this configuration. They cannot cross slip they do not have screw character. However, in order to reduce the energy, partial dislocations change the slip plane by exchanging point defects. In this process, the leading partial quickly put itself ahead the trailing one. When they reach the adjacent basal plane, they change again the slip plane to glide in it because basal slip system is the most favored. In this new basal plane another leading partial could be emitted, generating again another stacking fault area in this basal plane. The repetition of this process generates the appearance of bands with cubic structure that we have seen in the previous sections 3.2 and 3.3.

Every source can only emit only one leading partial in each basal plane, as it is shown in figure 15, the deformation of the material requires that the partial dislocations change successively the basal slip plane. This fact leads to a higher applied tension to keep the strain rate of the mechanical test. Consequently, the material does not exhibit the yield point and the elastic deformation is followed by the work hardening stage.

4. Conclussions

We have investigated the dislocation microstructure of silicon carbide 4H single crystals strained at around the transition temperature, whose value of 1030 °C was previously established by others authors. But in this work we have investigated a much wider temperature range (from 900 °C to 1300 °C). That allowed us to find that both mechanisms co-operate together from 1000 ºC to 1100 ºC, so that means that the transition temperature is actually a range comprised at least between this two temperatures. At high temperature regime, by WB-DF trace analyses using large-angle tilt we found that dissociation of basal dislocations take place by glide, where partials are separated by 32 ± 4 nm. These results have been corroborated by HRTEM observations.

Consequently, we obtained the stacking fault energy value in the basal plane is 20±5 mJ/m^2, which is in good agreement with both experimental and simulated results obtained by different authors. Since both partials slip together in this regime, glide dissociation has a neglect effect on mechanical properties. Dissociation of basal dislocations also takes place at the lower temperature regime, even at temperatures as low as 900 °C. However, in this regime the difference in mobility between the leading and the trailing partial seems to be so high that the later cannot follow the former and this one glide alone. Then, only leading partials are observed in micrographs. Nevertheless, here we found that leading partials have not all the same Burgers vector and also that they are different in character. Then, that indicates that not only the dislocation core composition, as previously reported, but also the dislocation character has a strong influence on the dislocation mobility. Thus, the combination of both factors finally decides which one is going to be the leading and the trailing partial after basal dissociation. This remarkably difference in mobility leads for one hand to a different mechanical behavior, characterized by a quick and strong work hardening, practically inexistent in the high temperature regime. On the other hand, it generates bands with 3C cubic structure inside the 4H-SiC matrix, whose amount decreases with temperature, and some especial fringes in WB micrographs, which can be also taken like an evidence of the low mechanism operation. From 1000 °C to 1100 °C dislocation microstructure is composed by a mixture of configurations we have observed in both high and low temperature regimes. Lastly, we also discuss about the influence of the dipole effect on the dissociation configuration.

Acknowledgements

We are grateful to M. Kelsch and U. Salzberger for their help in TEM specimen preparation. This work has been financially supported by the Ministry of Education and Science (Government of Spain) through the project MAT 2006-03068 and by the Junta de Andalucía (Spain) through the excellency project P05-0337-FQM.

References

[1] Miao MS, Limpijumnong S, Lambrecht WRL. Appl Phys Lett 2001; 79:4360.

[2] Iwata H, Lindefelt U, Öberg S, Briddon PR. J Appl Phys 2003;93: 1577.

[3] Samant AV, Hong MH, Pirouz P. Phys Stat Sol 2000;222:75.

[4] Pirouz P, Yang JW. Ultramicroscopy 1993; 51:189.

[5] Samant AV, Pirouz P. Int. J Refract Metals Hard Met. 1998;16:277.

[6] Fujita S, Maeda K, Hyodo S. Phil Mag A 1987;55:203.

[7] Ning XJ, Havey N, Pirouz P. J. Am. Ceram. Soc 1997;80:1645.

[8] Ravier J, George A. Rev Phys Appl 1987;22:1327.

[9] Pirouz P, Samant AV, Hong MH, Moulin A, Kubin LP. J Mater Res 1999;14:2783.

[10] Lagerlöt KPD, Castaing J, Pirouz P, Heuer AH. Phil Mag A 2002;82:2841.

[11] Zhang M, Hobgood HM, Demenet JL, Pirouz P. J Mater Rev 2003;18:1087.

[12] Okojie RS, Xhang M, Pirouz P, Tumakha S, Jessen G, Brillson LJ. Appl. Phys. Lett. 2001; 79:3056.

[13] Kuhr TA, Liu J, Chung HJ, Skowronski M, Szmulowicz F. J. Appl. Phys. 2002; 92:5863.

[14] Idrissi H, Lancin M, Douin J, Regula G, Pichaud B. Mater. Sci. Forum 2005; 483-485:299.

[15] Demenet JL, Hong MH, Pirouz P. Scripta mater. 2000 ; 43: 865.

[16] Castillo-Rodríguez M, Castaing J, Muñoz A., Veyssière P, Domínguez-Rodríguez A. Acta Mater 57 2009;57:2879.

[17] Hirth JP, Lothe J. New York: McGraw-Hill; 1968.

[18] Umeno Y, Cerný M. Phys Rev B 2008;77:100.

[19] Hong MH, Samant AV, Orlov V., Farber B., kisielowski C, Pirouz P. Deformation-induced dislocations in 4H-SiC and GaN, in: Mat Res Soc Symp Proc. 572 Mat Res Soc; 1999.

[20] Hong MH, Samant AV, Pirouz P. Phil Mag A 2000;80:919.

[21] Käckell P, Wenzien B, Bechstedft F. Phys. Rev. B 1994;50:17037.

[22] Cheng C, Needs RJ, Heine V. J Phy C 1988:21;1049.

[23] Castillo-Rodríguez M, Sigle W. Scripta mater 2009;62:270.

FIGURE CAPTIONS

Figure 1. Dislocation microstructure of 4H-SiC deformed by basal slip at 1300 ºC. Inserts taken under different g reflections show the stacking fault fringes and the extinction of each partial.

Figure 2. TEM micrograph of 4H-SiC deformed by basal slip at 1300 º C, showing the two basal dissociated dislocations that have been analyzed.

Figure 3. a) High resolution micrograph of 4H-SiC deformed by basal slip at 1300 º C. b) Stacking plane sequence besides the black arrow of figure 3.a.

Figure 4. TEM Micrograph of a 4H-SiC sample deformed by basal slip at 900 º C. (1, 2, 6, 7, 8 have **b**=1/3[01$\bar{1}$0], 5, 9, 10, 11 **b**=1/3[$\bar{1}$100], y 3,4 **b**=1/3[10$\bar{1}$0])

Figure 5. High resolution micrograph of 4H-SiC deformed by basal slip at 900 º C, showing 3C bands (B).

Figure 6. Magnification of one band from figure 5. Changes in the staking plane sequence are shown.

Figure 7. Dislocation microstructure of 4H-SiC deformed by basal slip at 1100 º C. Inserts on the right show the stacking fault fringes. The top central one displays some reactions between partial dislocations.

Figure 8. Scheme of the central insertion of figure 7 showing reactions between partial dislocations (**b**=1/3[$\bar{1}$2$\bar{1}$0], $\mathbf{b_1}$ = 1/3[$\bar{1}$100] and $\mathbf{b_2}$ = 1/3[01$\bar{1}$0] are in black, blue and red respectively.

Figure 9. Dislocation microstructure of 4H-SiC deformed by basal slip at 1000 ºC.

Figure 10. High resolution micrographs of 4H-SiC deformed by basal slip at 1100 ºC. 3-cubic bands (B) and dissociation processes (D) are observed.

Figure 11. Scheme of the dipolar configuration in figure 10.c, showing the repulsive (F^R) and attractive (F^I) forces between partials and the one due to stacking fault energy (F^γ).

Figure 12. High-resolution micrograph of the 4H SiC sample deformed by basal slip at 1300 ° C. Partials are marked by arrows, and the stacking plane sequence surrounding the black one is analyzed in figure 18.

Figure 13. Analysis of the stacking plane sequence on the left and the right side of the black arrow of figure 12.

Figure 14. Scheme of a Frank-Read source of basal dislocations, which is dissociated. After the emission of partial pair, the situation of the source becomes the original and therefore it is possible to emit more partial dislocations in the same plane.

Figure 15. Scheme of a Frank-Read source of basal dislocations, where only the leading partial (in blue) is emitted. After that, by exchanging point defects, both reach the next basal plane where again another leading partial can be emitted.

TABLES

Table 1. Distance d between partial dislocations for various electron beam orientations θ (angle between the electron beam and [0001] direction) of the basal dissociated dislocations 1 and 2 in figure 2.

Table 2. Distance h between partials and the angle β (between the stacking fault plane and [0001] direction) of the basal dissociated dislocations 1 and 2 in figure 2.

Table(s)

Dissociated dislocation 1	θ (°)	5 ± 2	15 ± 2	25 ± 2	35 ± 2	-8 ± 2	-18 ± 2	-28 ± 2
	d (nm)	32 ± 2	28 ± 2	26 ± 2	23 ± 2	31 ± 2	27 ± 2	25 ± 2
Dissociated dislocation 2	θ (°)	5 ± 2	15 ± 2	25 ± 2	35 ± 2	-8 ± 2	-18 ± 2	-28 ± 2
	d (nm)	33 ± 2	29 ± 2	28 ± 2	27 ± 2	33 ± 2	29 ± 2	27 ± 2

Table2

	β(°)	h (nm)
Dissociated dislocation 1	110 ± 15	32 ± 4
Dissociated dislocation 2	100± 15	33 ± 4

Figure1

Click here to download high resolution image

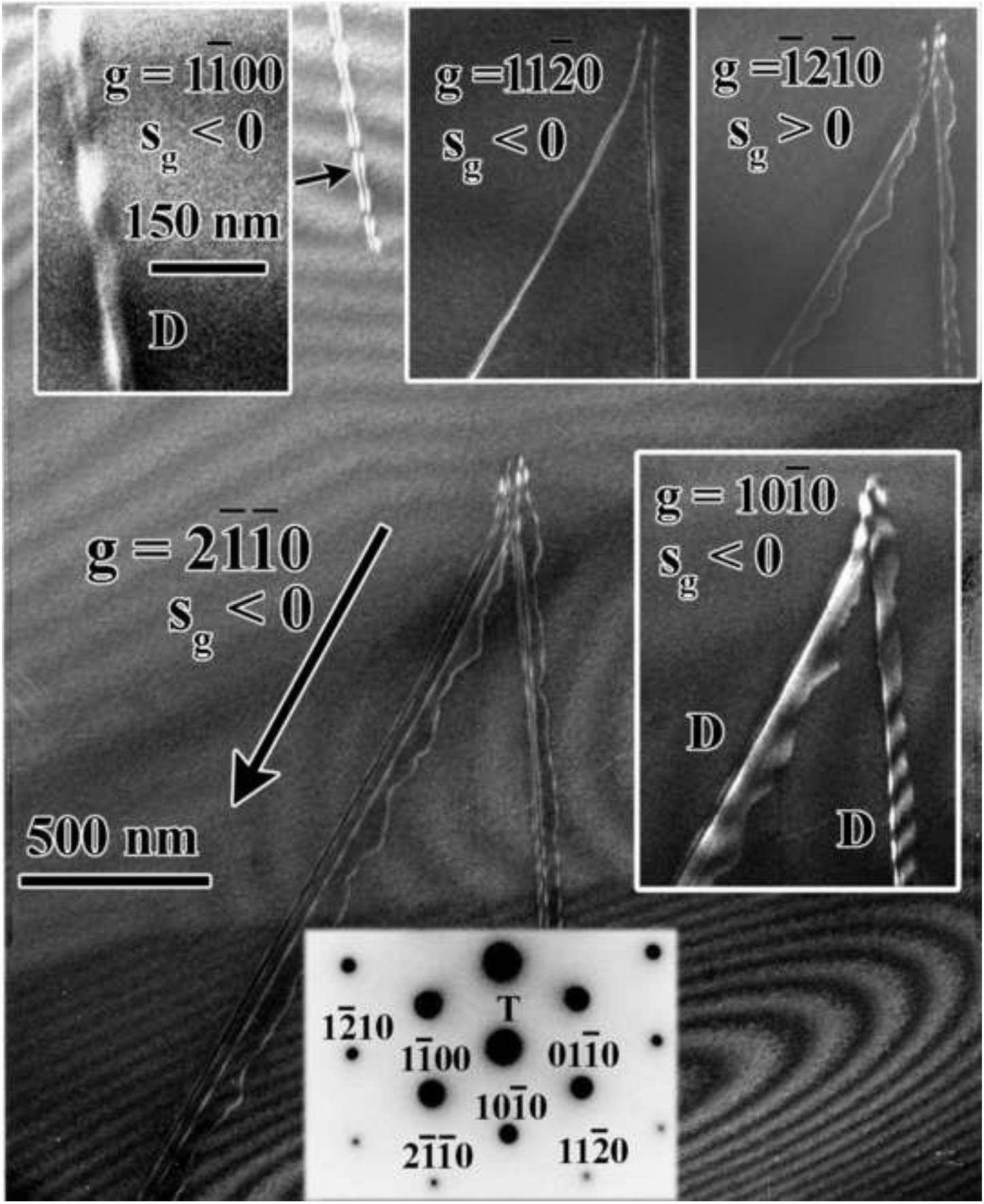

Figure2
Click here to download high resolution image

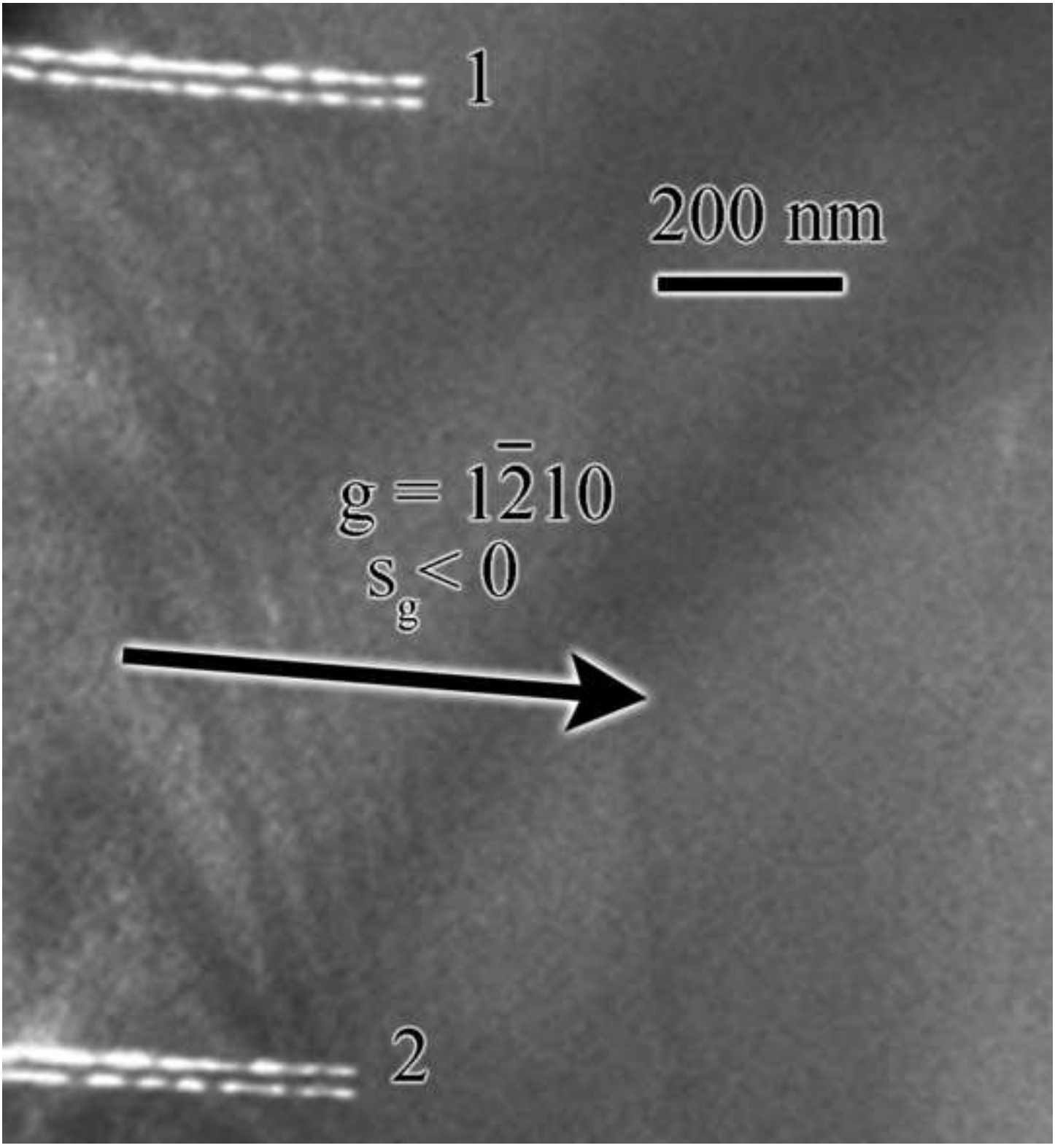

Figure3a
Click here to download high resolution image

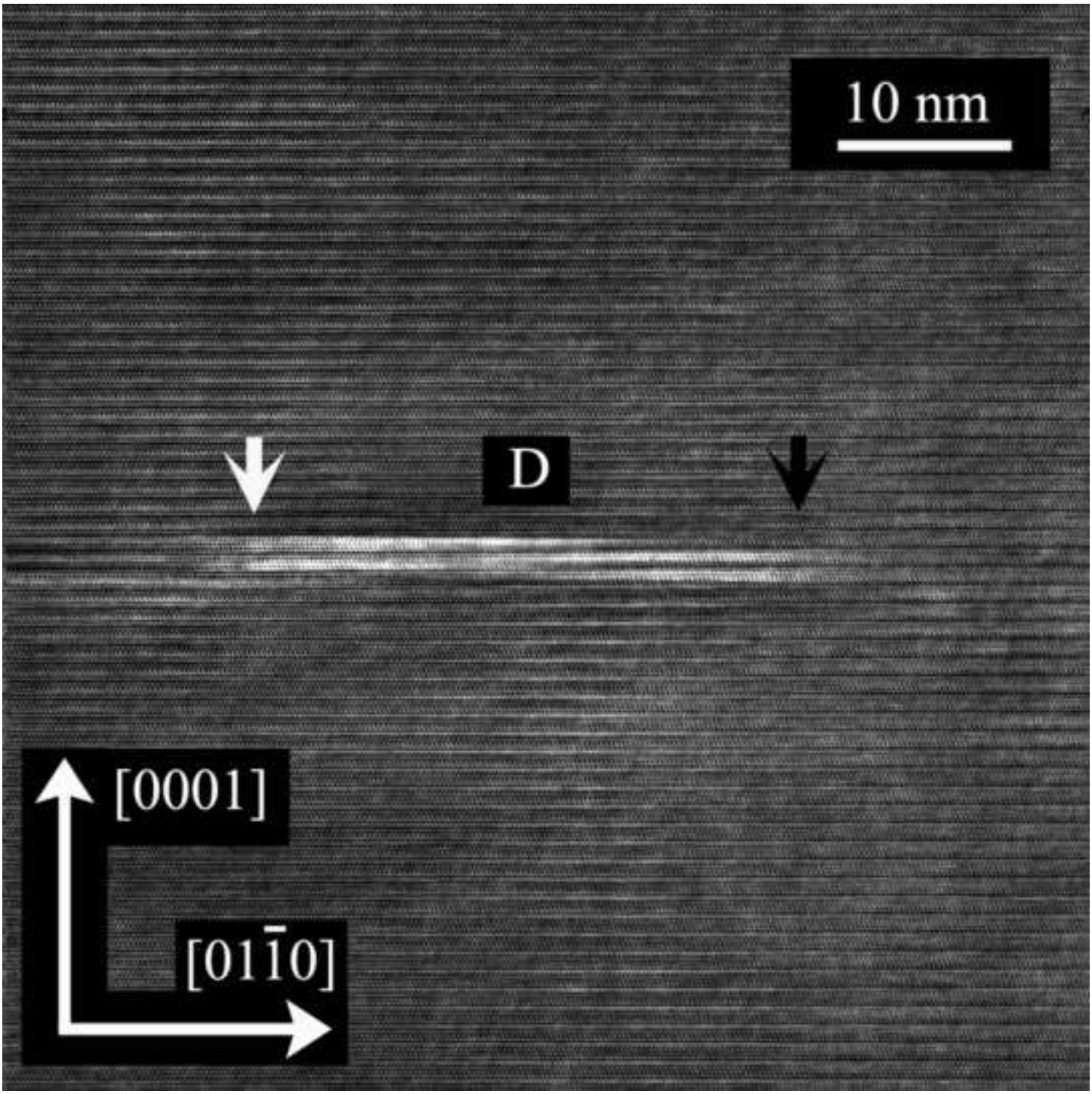

Figure3b

Click here to download high resolution image

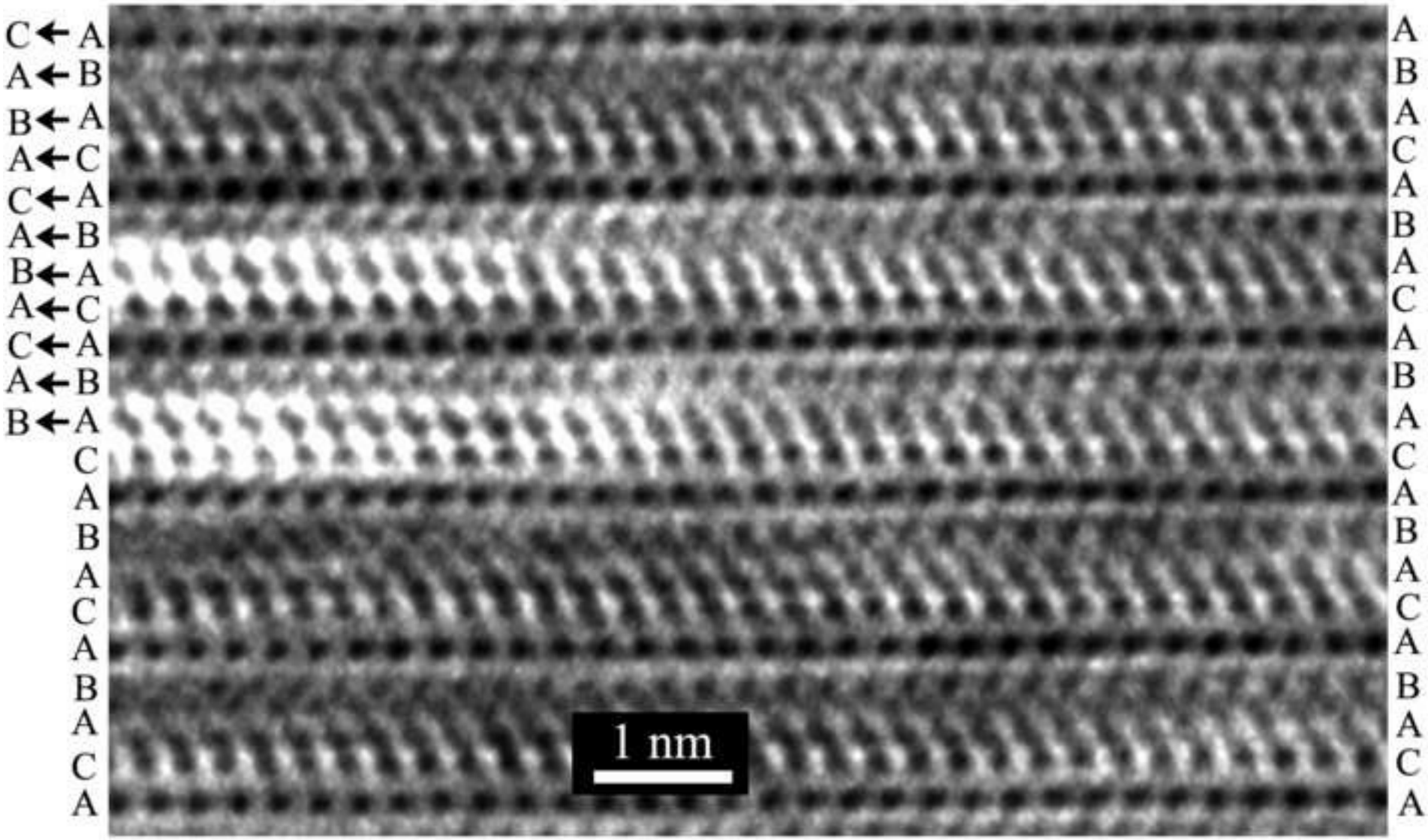

Figure4
Click here to download high resolution image

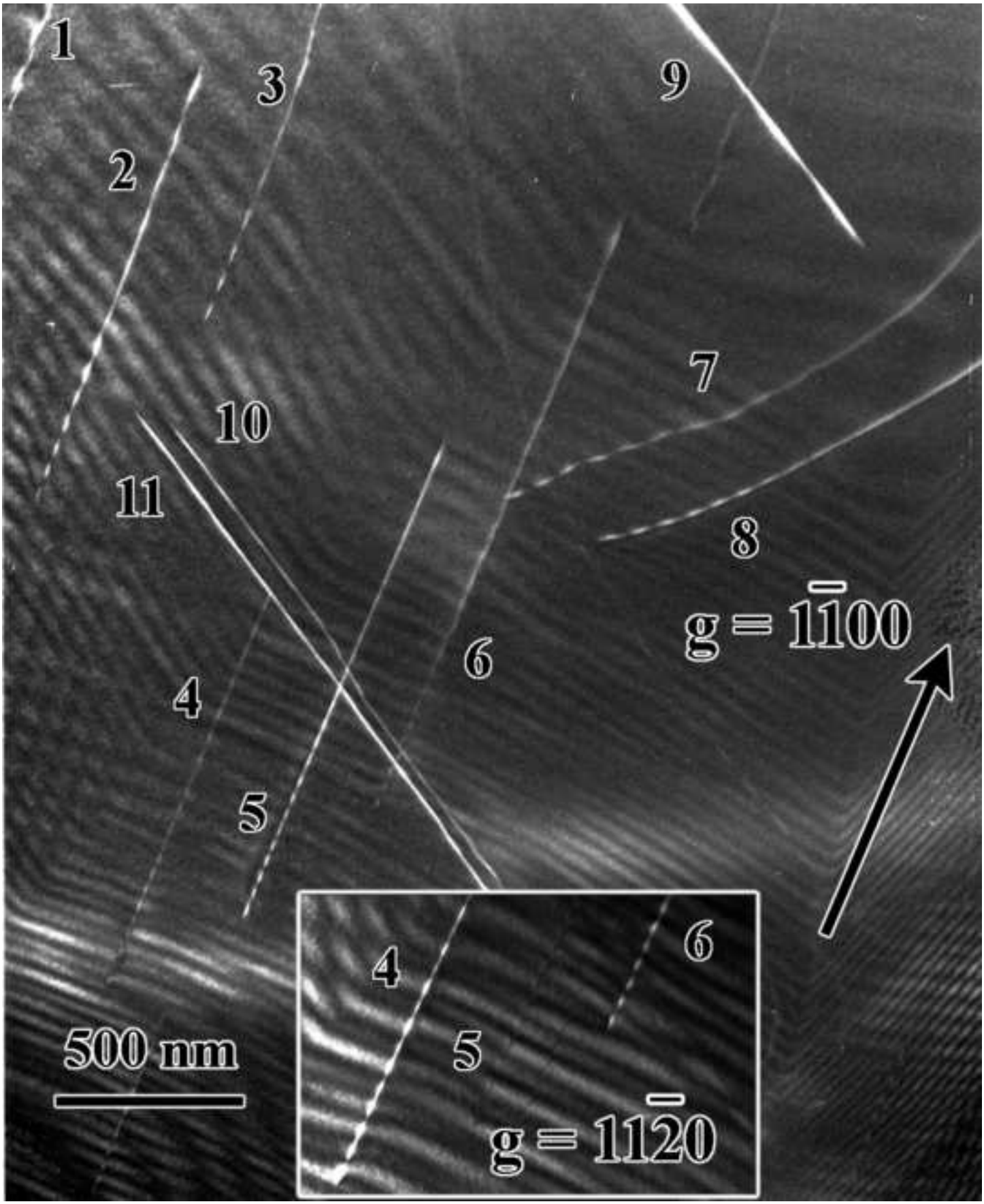

Figure5

Click here to download high resolution image

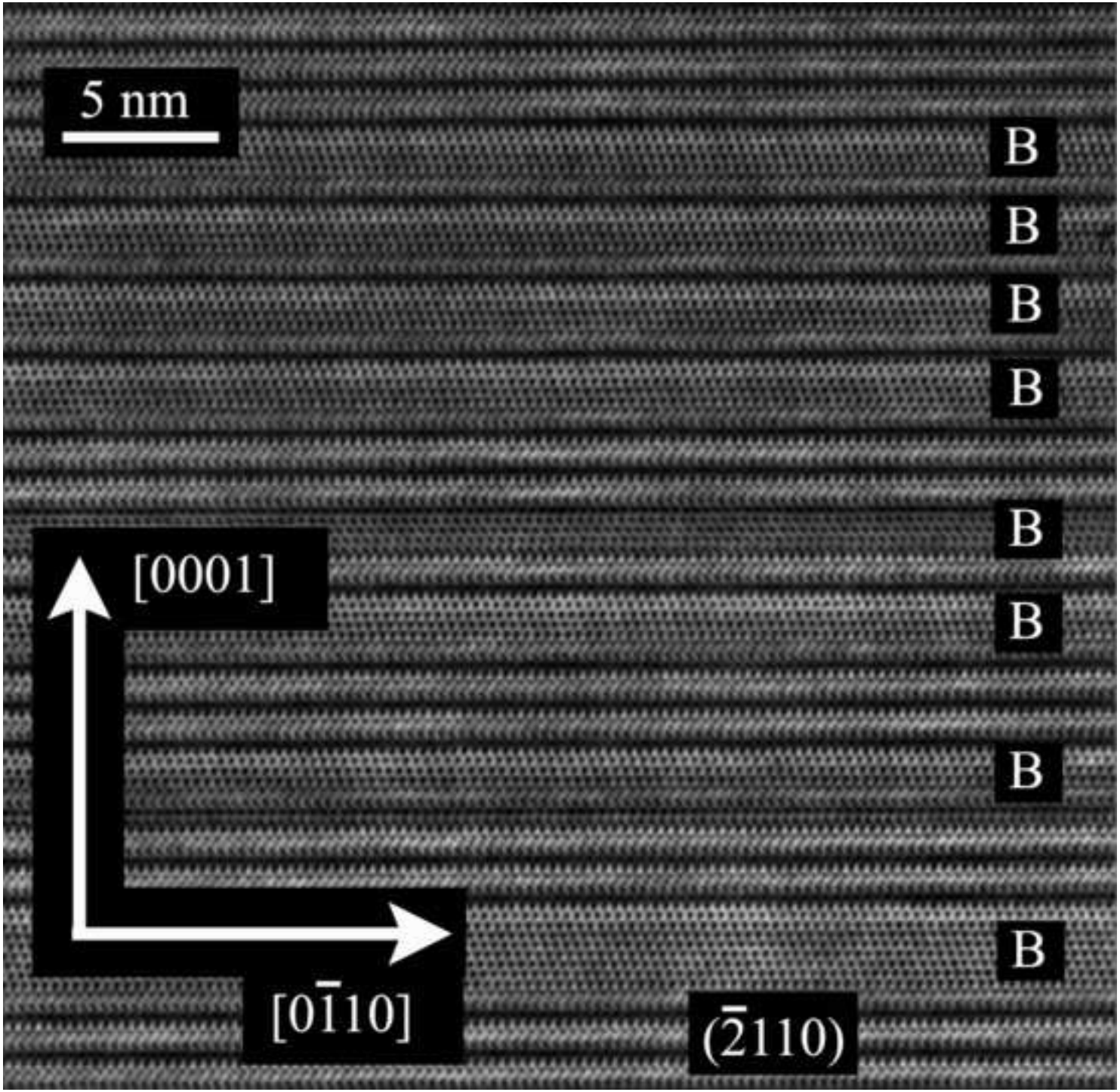

Figure6
Click here to download high resolution image

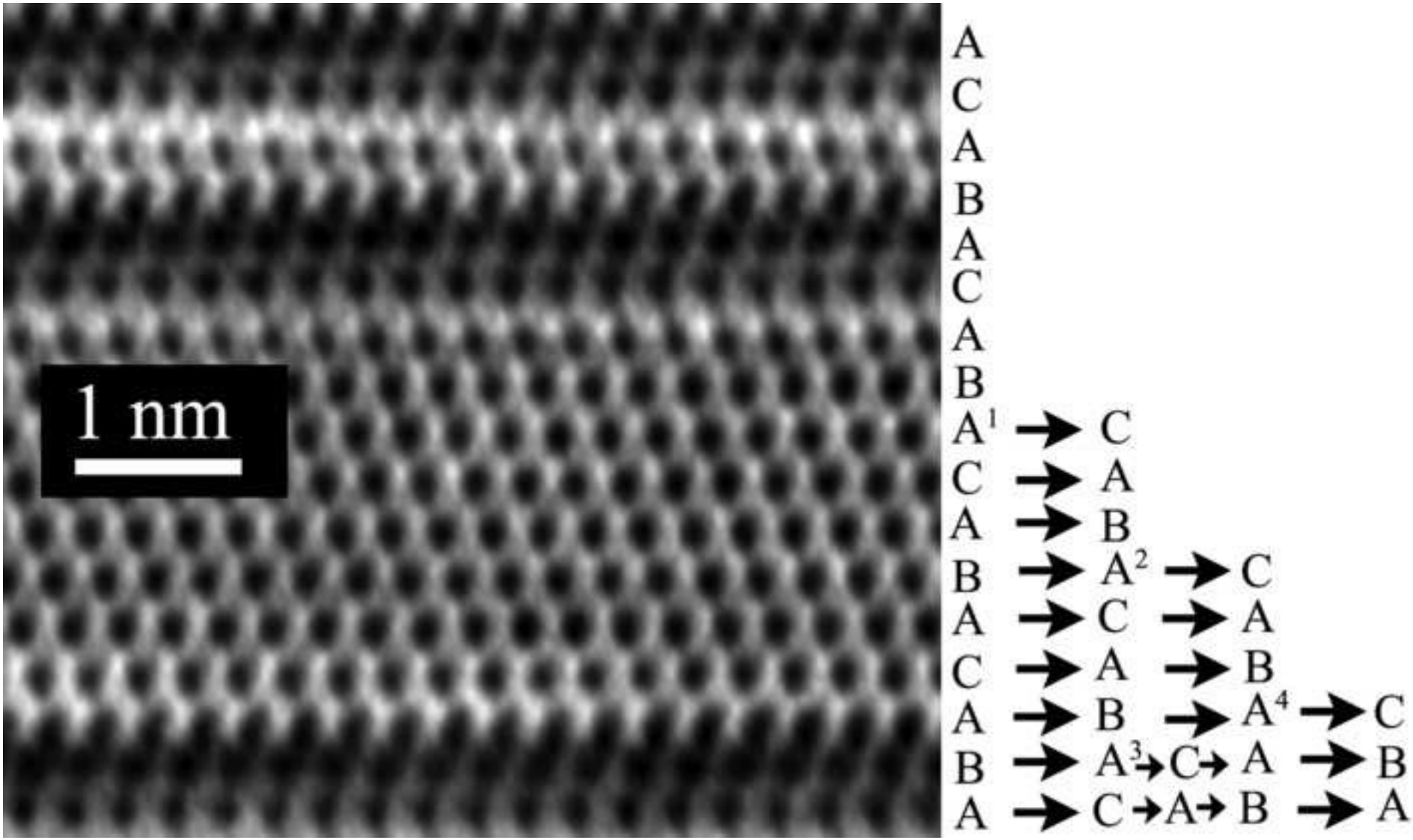

Figure7

Click here to download high resolution image

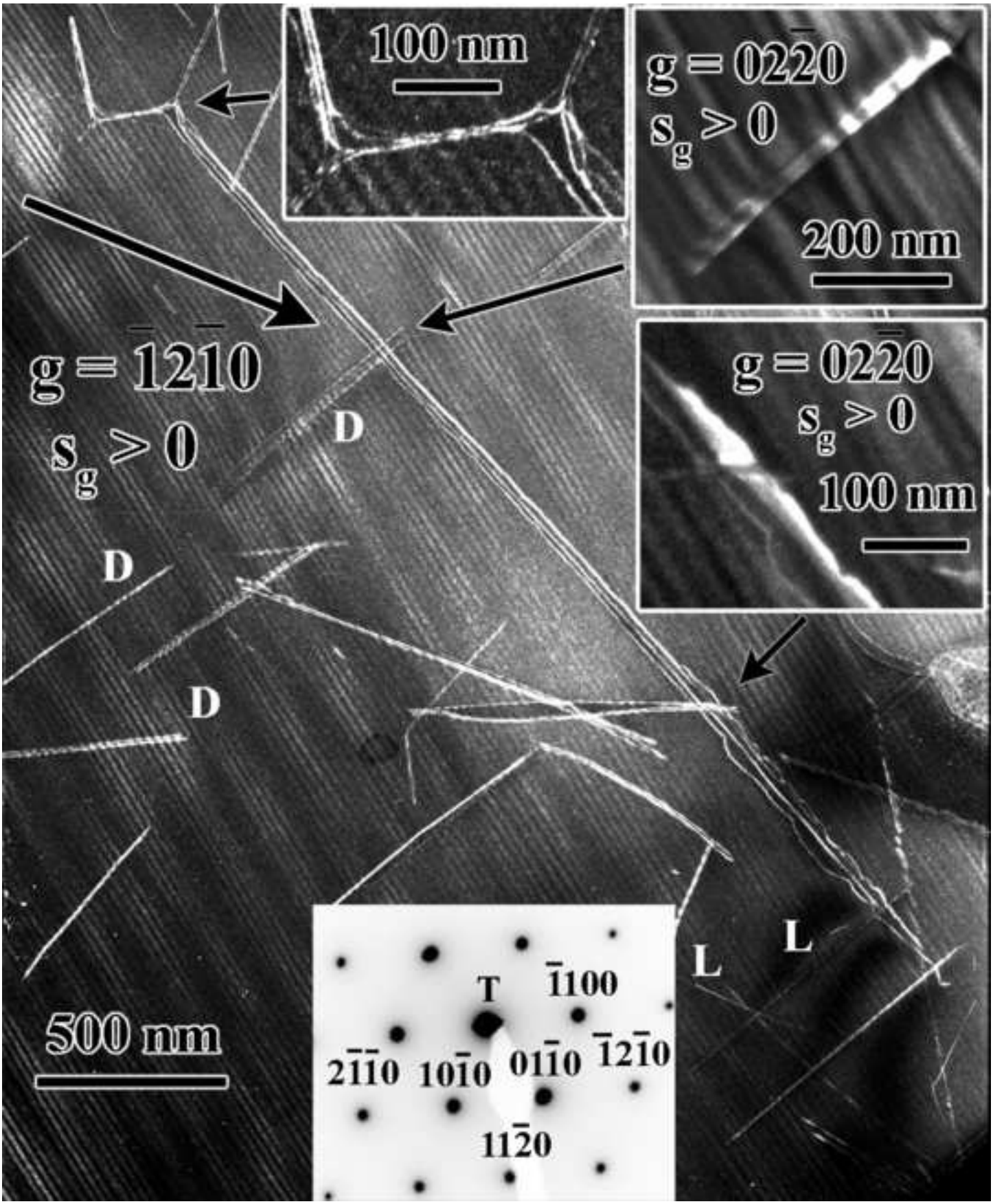

Figure8

Click here to download high resolution image

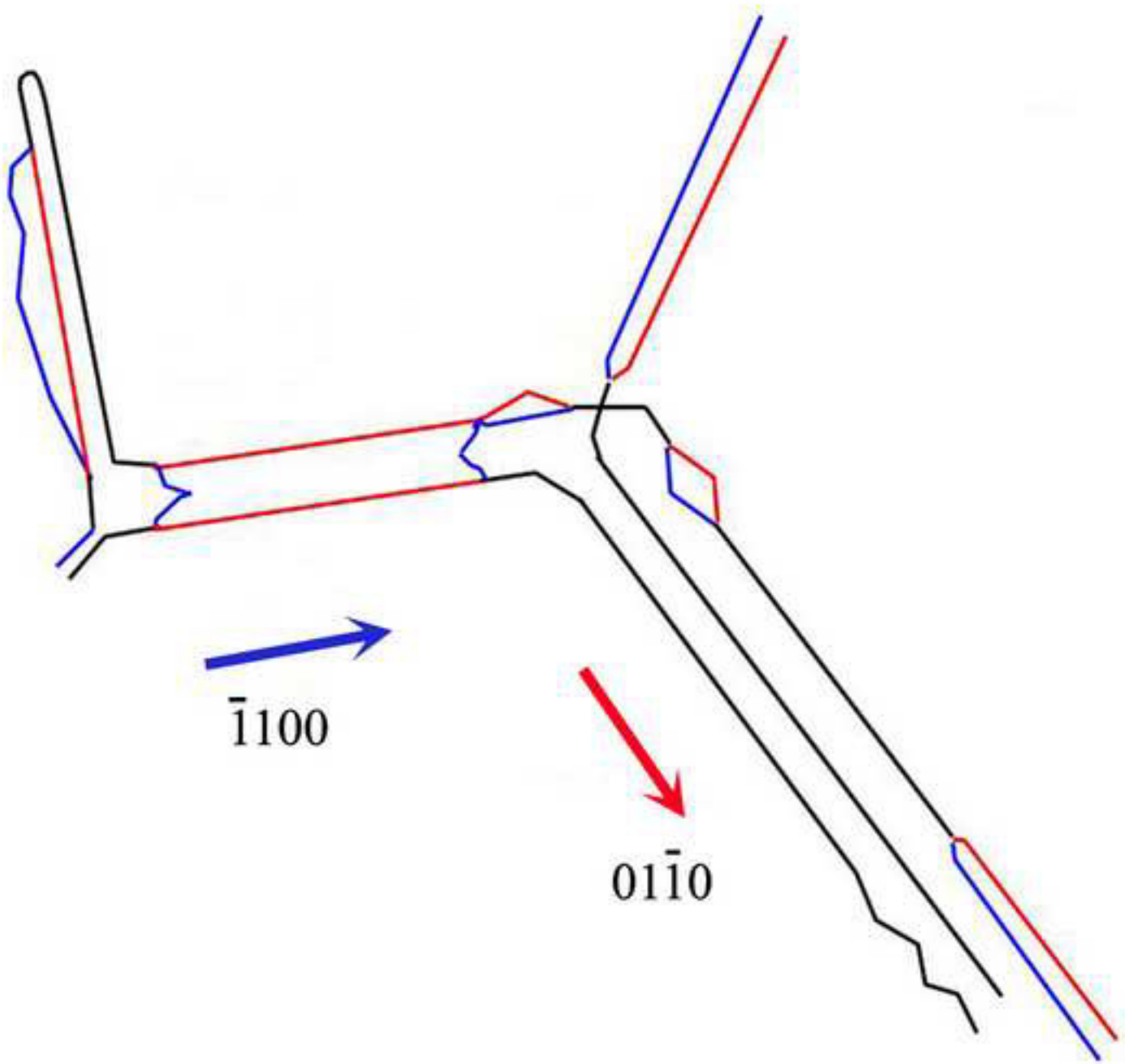

Figure9
Click here to download high resolution image

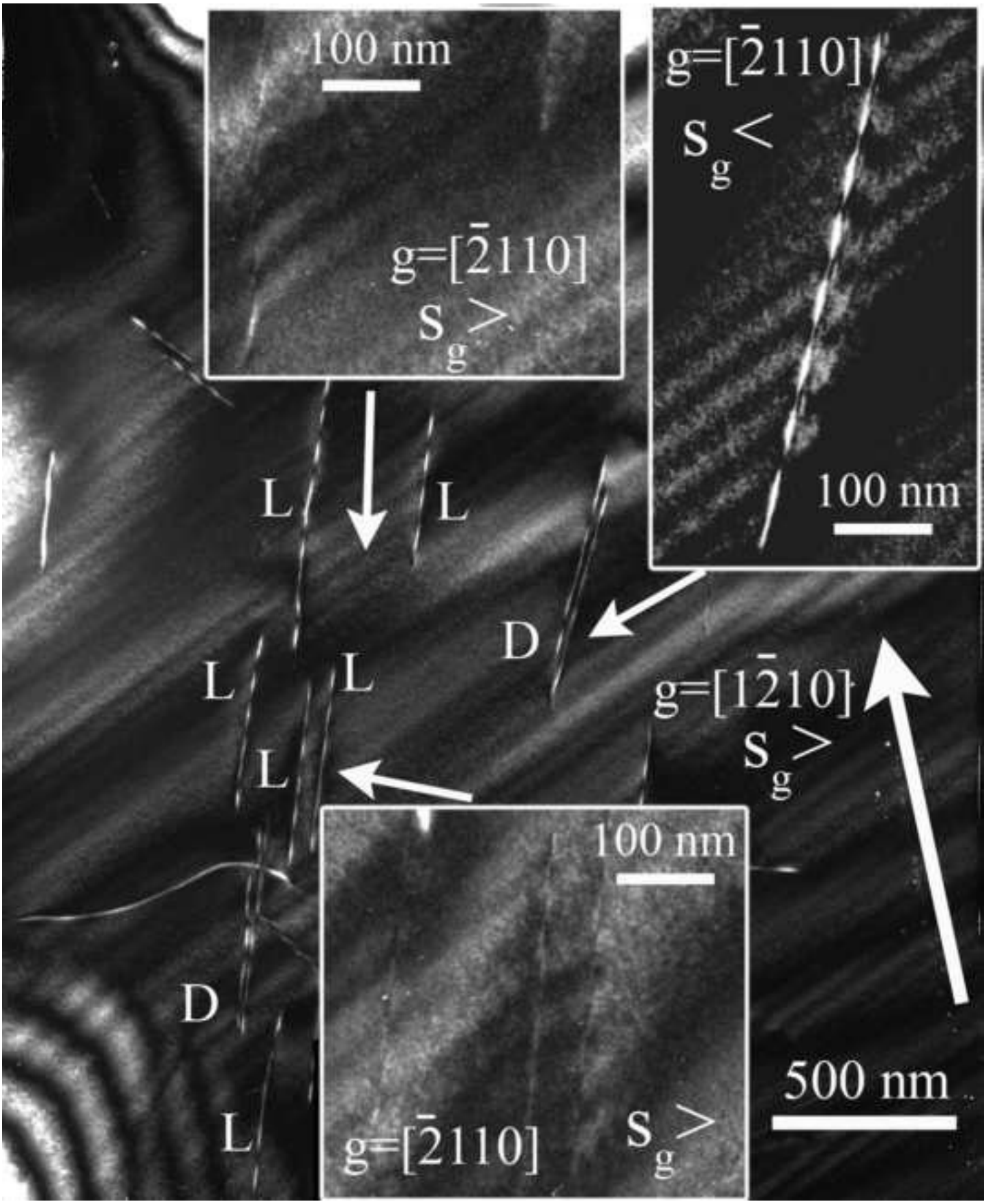

Figure10a
Click here to download high resolution image

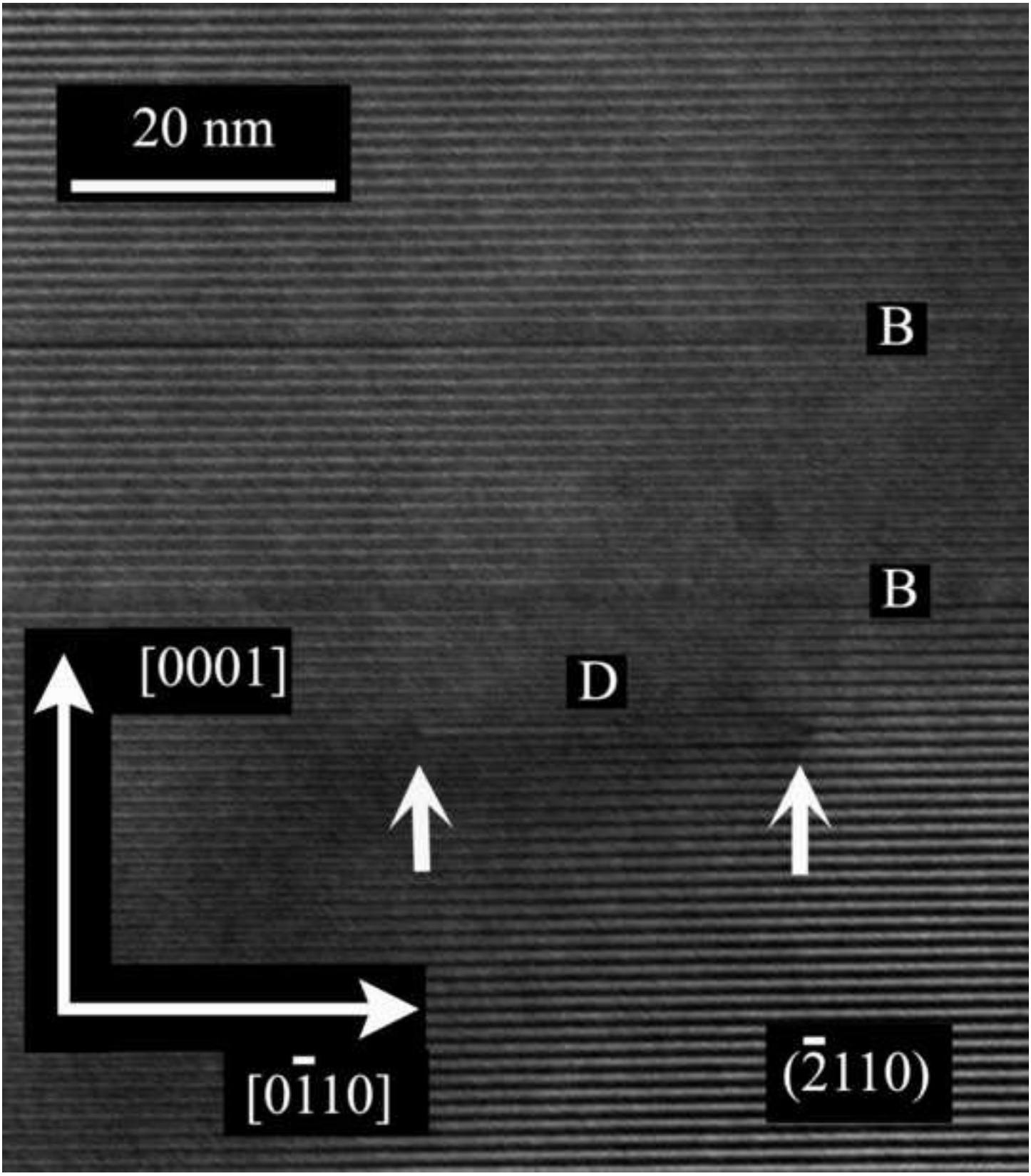

Figure10b
Click here to download high resolution image

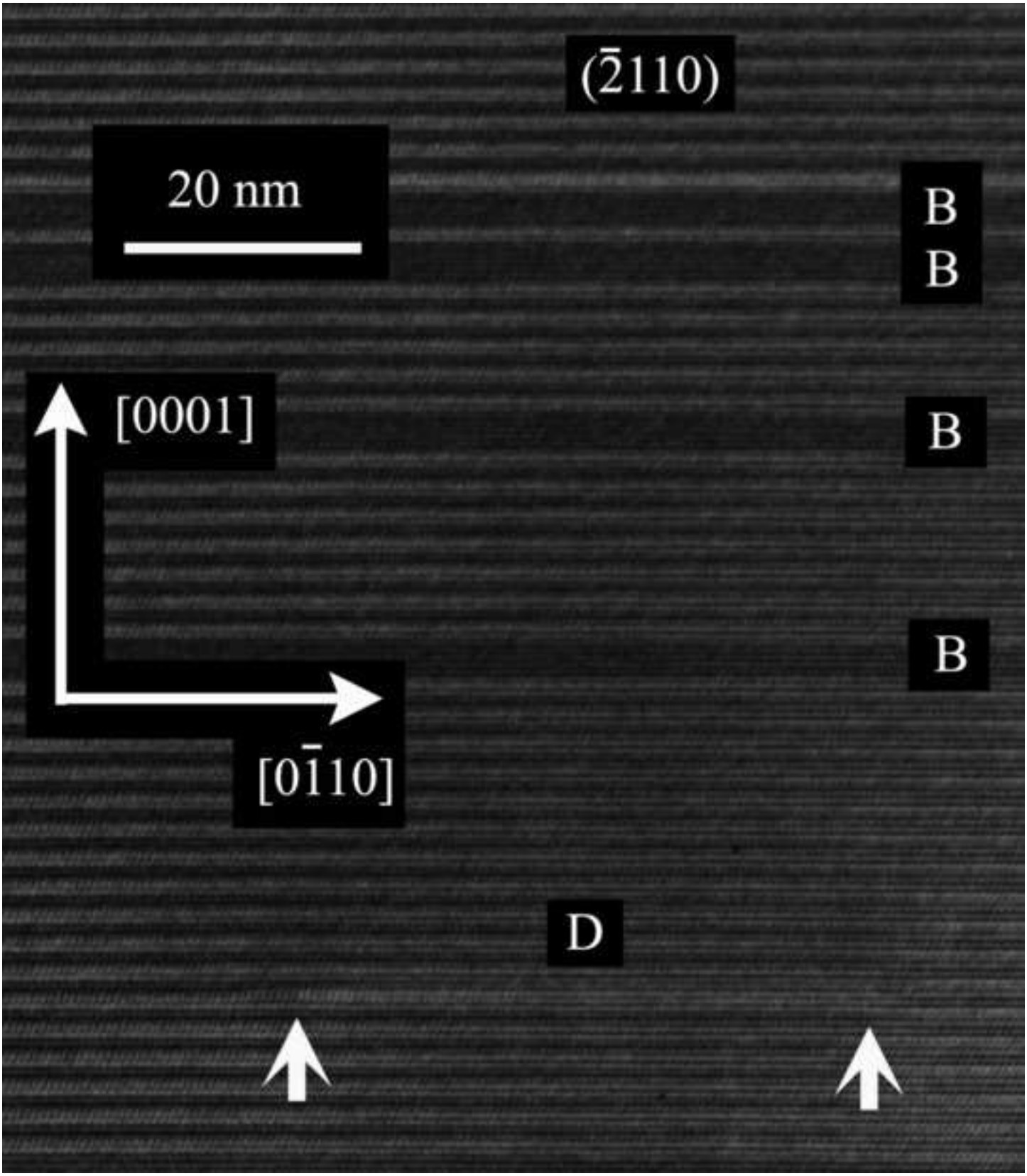

Figure10c
Click here to download high resolution image

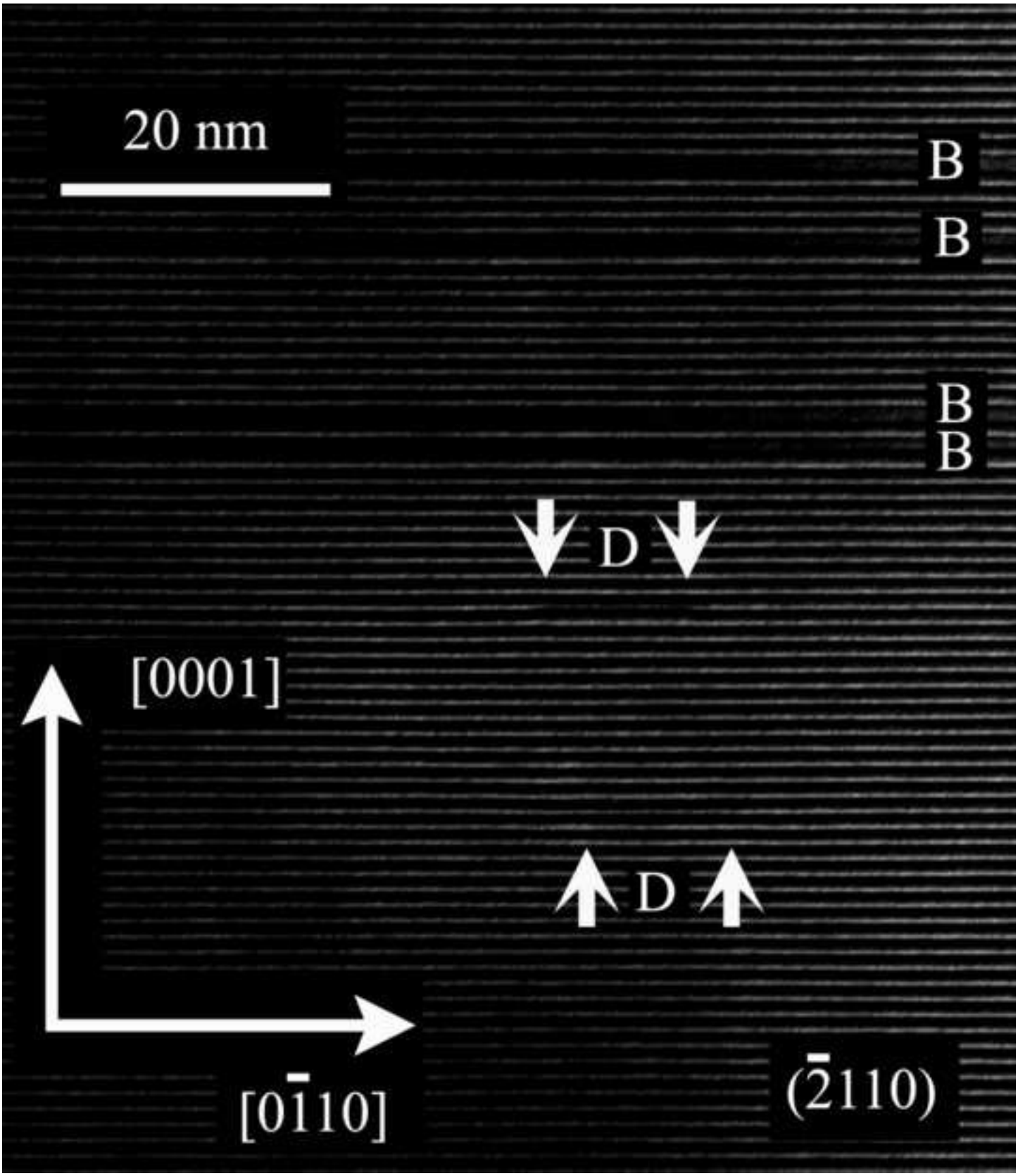

Figure11
Click here to download high resolution image

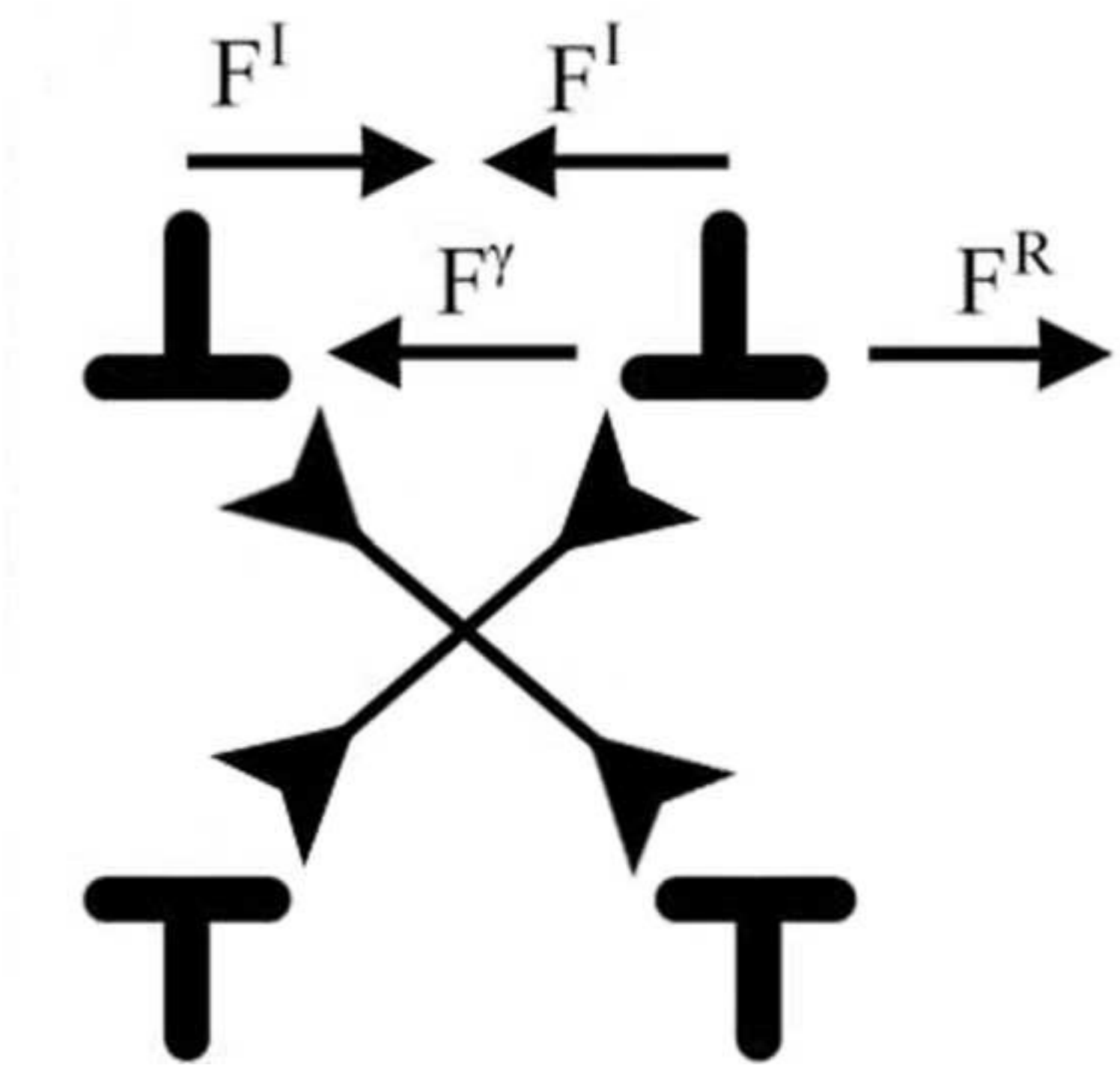

Figure12

Click here to download high resolution image

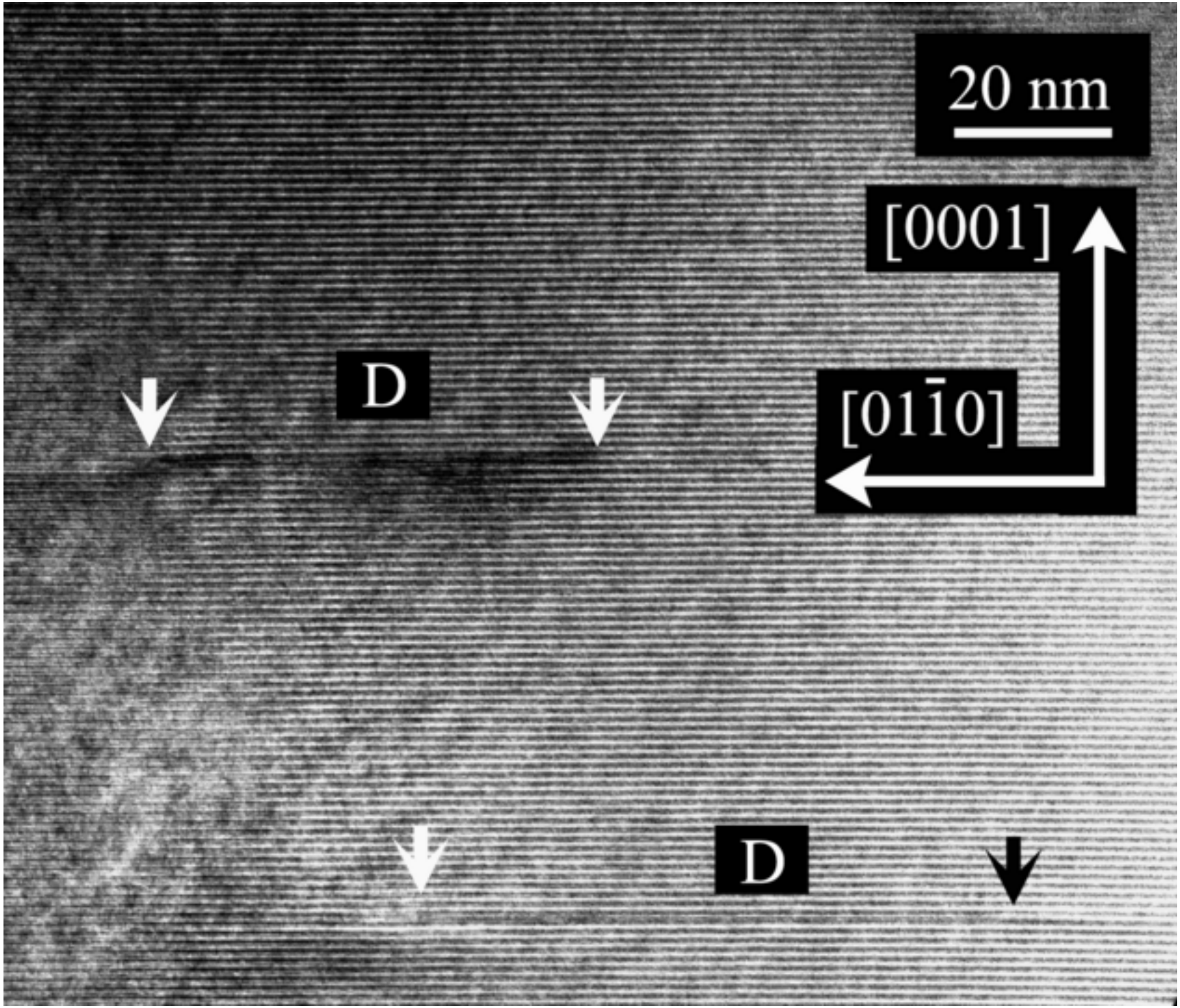

Figure13

Click here to download high resolution image

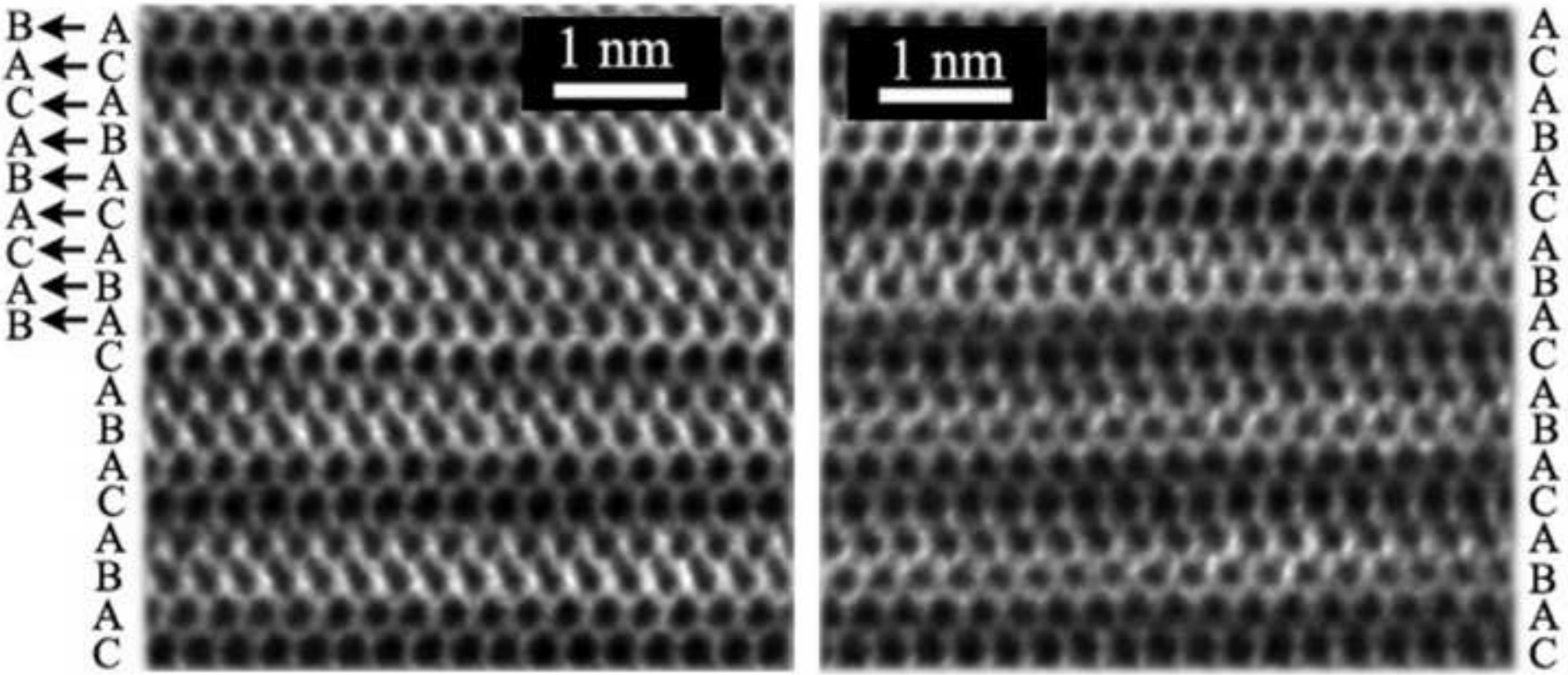

Figure14

Click here to download high resolution image

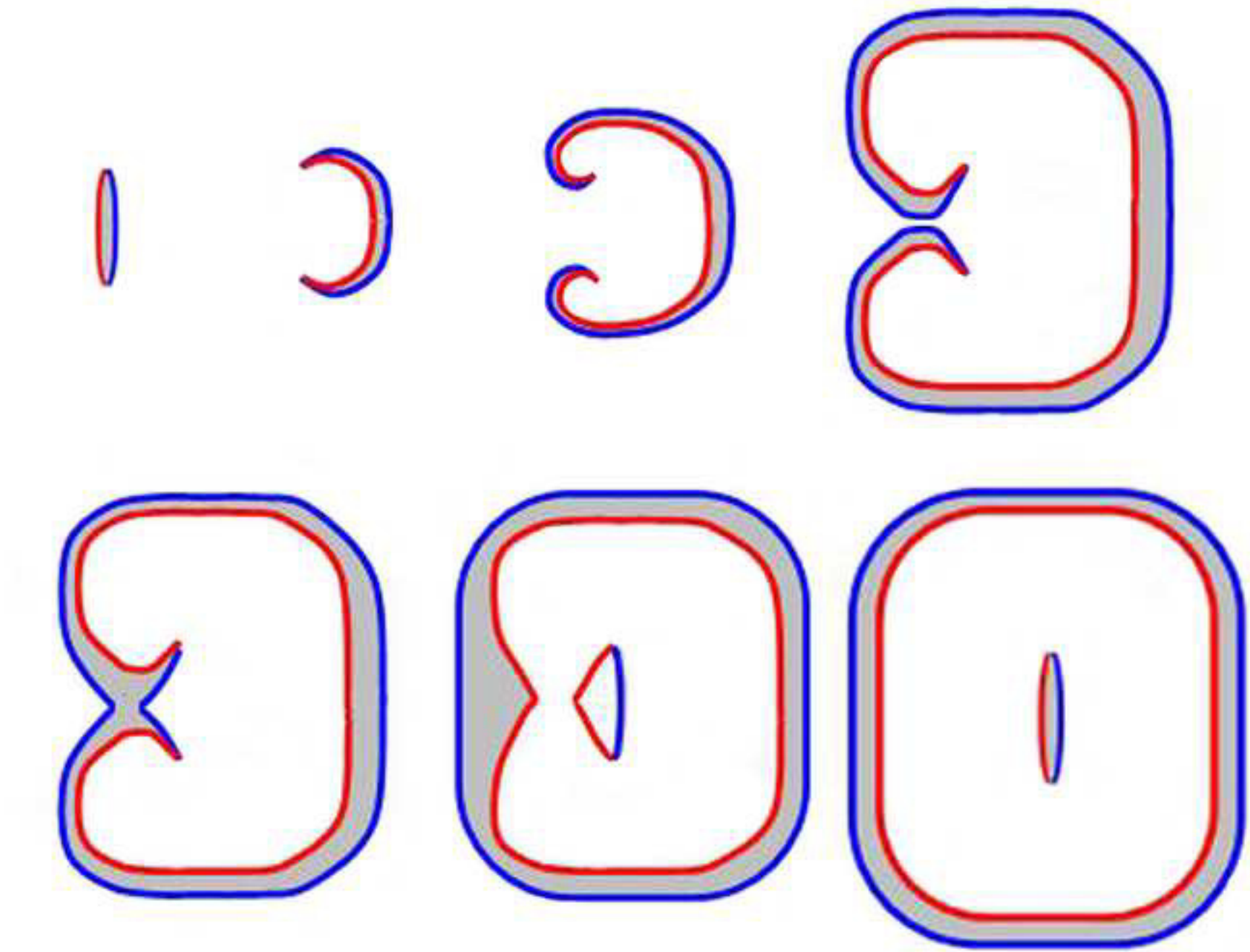

Figure15
Click here to download high resolution image